

Quantitative Assessment of Calibration Motion Profiles in Robotic-assisted Ultrasound System

Maarten Schoovaerts*, Ruixuan Li*, Kenan Niu and Emmanuel Vander Poorten

Abstract—3D ultrasound(US) reconstruction has grown quickly in preoperative disease diagnosis, intraoperative surgical navigation and postoperative treatment assessment. US image calibration is a crucial step to produce accurate 3D representations from 2D images. Several image calibration methods have been developed for freehand and robotic systems. During calibration, the scanning motions can vary a lot and typically have a large impact on the resulting calibration and subsequent reconstruction quality. However, the adopted calibration motions are not detailed extensively in previous studies. This complicates reproduction of the obtained results. Moreover, the influence of the different scanning motions on the calibration accuracy is hardly investigated. Therefore, it is difficult to devise optimal scanning motion profiles for automatic robotic ultrasound calibration. This paper studies calibration and reconstruction results with different motion profiles employed in robotic US image calibration. Then, the calibration procedure was performed with a sphere phantom. The performance of the calibration was validated by assessing the reconstruction quality on a 3D printed mock-up model with two quantitative measurements for the *geometric representation error* and the *3D localization error*. The geometric representation error of the reconstruction is within 1 mm by using the different combination of motion profiles. However, the 3D localization error changes with the various motion profiles. By using the proposed motion profile, the RMSE of the reconstructed model could be reduced to 2.18 mm.

Keywords: Motion profile, Ultrasound image calibration, Robotic control, 3D ultrasound reconstruction

I. INTRODUCTION

Reconstructed 3D ultrasound (US) volume could offer a non-radiative tool for clinicians with detailed geometric information of organs, tissues and anatomical structures [1]–[3]. The US image calibration is a crucial step for accurate 3D volume reconstruction from 2D images. Incorrect image calibration will cause inaccurate volume rendering and geometric distortion which could produce severe consequences, as surgeons' decision-making process could be hampered by it [4], [5].

There are several image calibration approaches and phantoms developed for the freehand and robotic-assisted systems [6]. Conventional freehand calibration is time consuming and labor intensive. Only a skilled operator can produce consistent and reliable calibration scanning. Different to it, robotic-assisted calibration is an alternative which provides automatic and stable probe manipulation. However, it requires a predefined motion profile before scanning.

In previous studies [7], it is already showed that the 3D reconstruction quality depend on motions profiles used during calibration. Thus, it is important to investigate the influence of the different scanning motions on the accuracy of US calibration. Subsequently, based on knowledge of the influence, optimal motion profiles could be devised for improving the quality of robotic scanning and reconstruction. Several researchers already looked into ways to improve the US calibration accuracy, both for freehand and robotic-assisted approaches [8]–[11]. The scanning motion profiles were typically utilized as combination of individual translation and rotation motion. Treece *et al.* designed a freehand calibration motion profile for the Cambridge phantom [8]. The profile was defined as a combination of individual motions along US probe coordinate, which are vertical motion, side-to-side rotation and front-to-back translation and rotation. The calibration was evaluated with 3D reconstruction and achieving a 0.65 mm mean error. However, the impact of the individual motions on the reconstruction was not discussed thoroughly. Besides, Rousseau *et al.* proposed a framework to quantitatively evaluate the freehand US image calibration methods [9]. In Rousseau's study, rotation motion and translation motion were separately performed during calibration. Then, the calibration outcomes were computed and validated with 3D volume reconstruction. Comparing with the volume of the CAD model, the results revealed that translation motion was better than rotation motion to obtain accurate US image calibration. However, the combined motion profile was not investigated and evaluated. Based on the aforementioned freehand studies, two robotic approaches were implemented for US image calibration [10], [11]. Summarized from conventional freehand manipulation, Li *et al.* proposed a robotic calibration motion profile for the sphere phantom [10]. During scanning, the US probe was aligned with sphere center and tilted between ± 30 degree around phantom X and Y axis. Then, the US probe was translated 10 mm at the positions of ± 30 degree along probe Z axis. Aalamifar *et al.* also designed a robot motion for calibration scanning. The profile was defined as translation motion along the lateral and the elevation axis of US probe [11]. Although, the studies introduced the calibration motion profile with detail, the influence of motion profiles was not investigated extensively. In summary, for different calibration approaches, the scanning motion profile could vary greatly. But in previous studies, these motions were not analysed in depth or communicated which may affect the reproducibility of the work.

To best of our knowledge, this is the first paper inves-

* These authors contributed equally to this work.

M. Schoovaerts, R. Li, K. Niu and E. Vander Poorten are with the Department of Mechanical Engineering, KU Leuven, Belgium (email: maarten.schoovaerts@kuleuven.be)

tigating the influence of motion profiles in US image calibration. This work devises an effective calibration approach for robotic-assisted US system with a sphere phantom. It studies the influence of different robotic motion profiles on the overall calibration accuracy. The paper provides a list of scanning motions and a quantitative analysis of the different motion profiles and the impact on calibration and US reconstruction accuracy. From this, an optimal scanning trajectory for calibration of a robot-assisted US system is derived.

The paper is built up as follows. The materials and methods employed in this work are introduced in Sec.II: the scanning motion profiles are introduced in SubSec.II-B, performance criteria in SubSec.II-C and the experimental setup in SubSec.II-D. Section III summarizes the main results, which are discussed in Sec.IV. Finally, conclusions and directions for further work are discussed in Sec.V.

II. MATERIALS AND METHODS

A. US image calibration

The goal of US image calibration is to find the unknown transformation (${}^R_{US}\mathbf{T}$) from the US image to the robot end effector and scaling transformation \mathbf{T}_s , containing scale factors s_x, s_y , from the US image pixels to a metric unit of length. In order to find these unknowns, the following equation is used:

$$\begin{bmatrix} p_x \\ p_y \\ p_z \\ 1 \end{bmatrix} = {}^Ph_B\mathbf{T} {}^B_R\mathbf{T} {}^R_{US}\mathbf{T} \begin{bmatrix} s_x u_r \\ s_y v_r \\ 0 \\ 1 \end{bmatrix} \quad (1)$$

The equation describes the target point in the robot base coordinate, termed ${}^B_{Ph}\mathbf{T}$. Fig. 1 illustrates a schematic overview of the relevant transformations. Note that all points are expressed in homogeneous coordinates. For the US image calibration in this paper, the target points (u_r, v_r) correspond to the center of the sphere phantom. Sphere phantoms are commonly used for US image calibration, as they are easy to manufacture and deploy [12]. During scanning, the center of the sphere can be positioned and aligned in the US image plane. Moreover, the sphere's contour, and thus its centre, can be easily segmented from 2D US images using image processing.

However, when using a sphere phantom, the accuracy of image calibration depends on how accurate the center point can be identified on the US images. Therefore, the US probe is required to align with the center of the sphere regardless of the US probe's position and orientation when performing a calibration procedure. Benefiting from robotic position control, we applied the following two steps to ensure continuous US image plane alignment with the sphere center. Firstly, the sphere phantom and corresponding center point is aligned with the US image plane by hand when the robot and US probe are in a initial, stationary position as shown Figure 1. Secondly, the robot performed motions, which are described in section II-B, starting from the initial position.

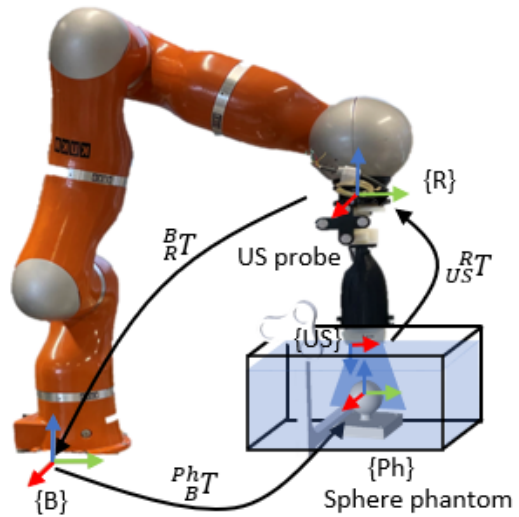


Fig. 1. Overview of experimental setup and transformations between each coordinate. ${}^B_R\mathbf{T}$ is the transformation from robot end effector to base coordinate, ${}^R_{US}\mathbf{T}$ is from US image to robot end effector coordinate and ${}^Ph_B\mathbf{T}$ is from base to sphere phantom coordinate.

In order to obtain the target point (u_r, v_r) from the 2D US images, image processing is used according to a previous study [10]. Firstly, a gaussian filter and thresholding was applied to blur the image reducing white spike noise. Subsequently, canny edge detection and Least squares approach was applied to segment the upper contour and estimate the center of circle with RANSAC to filter outliers. Since the target point is considered as the origin of the phantom, p_x, p_y and p_z can be set to zero. Therefore $\mathbf{p} = [0, 0, 0, 1]^T$, when capturing n images, this results in minimizing the following equation:

$$f(\mathbf{p}) = \sum_{i=1}^n | {}^Ph_B\mathbf{T} {}^B_R\mathbf{T} {}^R_{US}\mathbf{T} \mathbf{T}_s \mathbf{p}_r | \quad (2)$$

B. Robotic scanning motion

1) *Individual Motions*: Prior to the robotic US image calibration, a camera-to-robot calibration was performed by a point-to-point rigid registration method [13]. This procedure was implemented to calculate the transformation between camera coordinate and robot coordinate. Then the pose of the sphere phantom was converted into the robot coordinate for calibration scanning. During scanning, position control with eTaSL, expressiongraph-based Task Specification Language [14], was implemented to keep the US probe always aligning with the target point.

At the beginning, the US probe was moved close to the phantom and initially aligned with the target point in vertical direction. Subsequently, the probe started scanning twelve predefined motion profiles shown in Fig. 2 and Table I. While finishing each motion, the US probe returned to the initial position before initiating the next motion.

During scanning, US images and corresponding poses of robot end effector were stored separately for each individual motion simultaneously. However, the translation motion

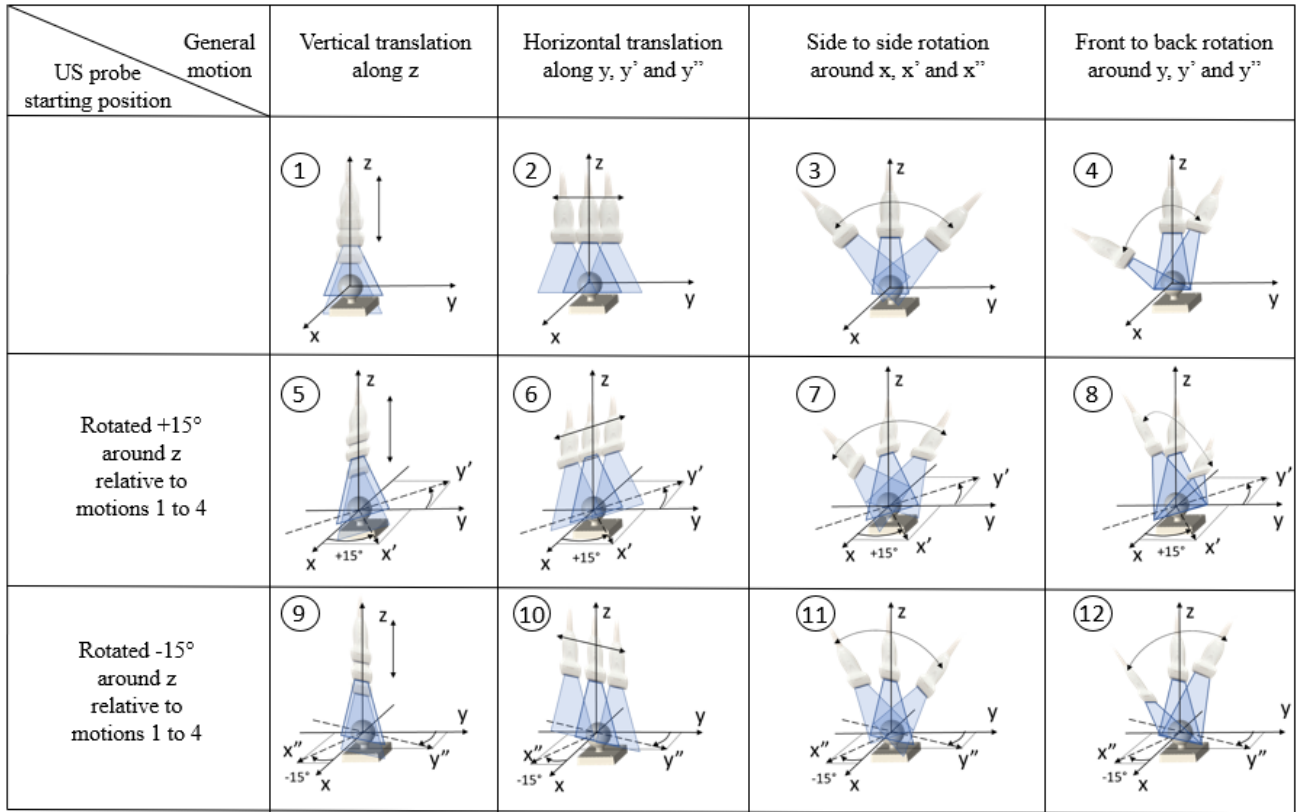


Fig. 2. Individual motion profiles for image calibration. The scanning motion is based on the defined axes from the sphere phantom.

along the x axis will not be performed as an individual scanning motion. This x-axis is aligned in a direction perpendicular to the US-beam. Hence, given the limited thickness of the US-beam, movement of the US probe along the x-axis would make the center of sphere quickly disappear from the US image leading to wrongly segmented sphere centers.

TABLE I
MOTION RANGE OF INDIVIDUAL MOTIONS

Motion type	motion range
Vertical translation	± 15 mm
Horizontal translation	± 15 mm
Side to side rotation	$\pm 20^\circ$
Front to back rotation	$\pm 20^\circ$

The motion ranges were set according to the dimensions of sphere phantom. Meanwhile, the ranges would also ensure that there is scattered movement of target points in the 2D US images without collision with the phantom. Besides, the speed of the probe motion is slow to eliminate influence of latency. The latency between US images and US probe location data results in imperfect synchronization and inaccurate calibration outcomes. This can either be solved by temporal calibration or by slow and stable probe motion. Therefore, the scanning speed of US probe tip was set as 1.5 mm/s for translation and 0.075 rad/s for rotation, respectively.

2) *Motion Profiles*: Making use of a single individual motion is insufficient to obtain accurate and precise calibration outcomes. Therefore, the proposed individual motions

of Fig. 2 were selected and combined to generate ten different motion profiles as shown in Table II. One data point corresponds to a single segmented US image with corresponding probe's pose. Then, the generated different motion profiles were processed to compute the calibration outcomes. The impact and influence on the calibration accuracy was analyzed by assessing the reconstructed results.

TABLE II
CALIBRATION MOTION DESIGN

Motion group	Motion profile	Utilized individual motions	Data points
I	1	1 to 2	1200
	2	5 to 6	1200
	3	9 to 10	1200
II	4	1 to 4	2000
	5	5 to 8	2000
	6	9 to 12	2000
III	7	1 to 8	4000
	8	1 to 4 and 9 to 12	4000
	9	5 to 12	4000
	10	1 to 12	6000

The calibration outcomes were computed by least square approach with Eq.2. The result was not sensitive to the sequence of processed data. Thus the order in which the motions were performed for each motion profile did not contribute to the final calibration outcomes.

C. Evaluation Criteria

The precision of US image calibration was assessed via repeated calibrations. However, the calibration outcomes would not directly provide quantitatively measurements. Thus, the calibration was measured by using reconstruction against the ground truth [15]. After computing transformation matrices and scale factors for the various motion profiles, the calibration results, and thus different motion profiles, were validated by 3D US reconstruction with a custom designed 3D printed mock-up model.

1) *Geometric Representation Error*: The first criterion evaluates how the geometric characteristics, i.e. size and shape, of the reconstructed model correspond to the mock-up model. The deviation between the reconstructed model and mock-up CAD model is referred to as the "geometric representation error". Since the geometric representation error does not depend on where the reconstructed model is located in space, but only on the geometry of reconstruction, the reconstructed point cloud can be aligned with the ground truth. For this purpose a simple registration can be conducted where we search for the transformation (\mathbf{R}, \mathbf{t}) to match the points in reconstruction P to the ground truth Q while m is the number of point. This process can be realized by using an iterative closest point algorithm (ICP) and is often used in medical image analysis [16]. This is done by minimizing the following equation:

$$f(\mathbf{R}, \mathbf{t}) = \frac{1}{m} \sum_{i=1}^m \| \mathbf{q}_i - (\mathbf{R}\mathbf{p}_i + \mathbf{t}) \|^2 \quad (3)$$

The ICP algorithm iterates until the error (i.e. the RMSE of Euclidean distances between reconstructed point cloud and ground truth) converges. Meanwhile, the mean error and standard deviation is calculated to present the difference between reconstructed model and CAD model.

2) *3D Localization Error*: In previous studies, the localization of reconstructed model was not evaluated comprehensively. However, the localization accuracy of reconstructed model is crucial which would influence the spatial relation with related instruments in the same coordinate system. Thus, the second criterion, the "3D localization error", is employed to assess whether the reconstructed point clouds locate at the actual 3D position of the phantom in the robot coordinate frame. This is realized by comparing the reconstructed points to the closest points in ground truth, which is obtained by the optical camera and converted into the robot coordinate frame. The results were calculated as point to point distances with RMSE, mean and standard deviation.

The number of reconstructed points could also influence the results. In order to compare the difference between similar motion profiles (e.g. *I*, *II* and *III*), the average value of RMSE, mean error and standard deviation for geometric representation and localization error was calculated. Where n is the number of points in the point cloud and N is the number of tests.

$$RMSE_{avg} = \sqrt{\frac{\sum_{i=1}^N (n_i \cdot RMSE_i^2)}{\sum_{i=1}^N n_i}} \quad (4)$$

$$\sigma_{avg} = \sqrt{\frac{\sum_{i=1}^N \sigma_i^2}{N}} \quad (5)$$

D. Experimental Setup

To achieve fully automatic scanning, a lightweight robotic arm (KUKA Robot LWR, Augsburg, Germany) was employed to manipulate a 7.5MHz linear US transducer (Sonosite, FUJIFILM, USA). A frame grabber (Epiphan Systems Inc. Palo Alto, Canada) was used to record the US images at a rate of 30Hz. Besides, to register the phantom pose in robot coordinate, an optical tracking system (FusionTrack 500, Atracsys, Switzerland) was integrated and operated at 335 Hz. A custom designed US probe holder was assembled at robot end effector and defined in Unified Robot Description Format (URDF) for robot control. To control the robot, OROCOS (Open Robot Control Software) was integrated and used to communicate with the robot arm at 1 kHz. In addition, a PC workstation was used for data acquisition and processing.

Two models, the calibration sphere phantom and mock-up model, were designed and 3D printed with polylactide. Before the models are scanned with the US probe, they were submerged in a water tank. The sphere phantom was made of a 30 mm diameter sphere. The diameter of the sphere was set to be able to capture a full contour of the phantom by using the linear US probe. The 3D printed sphere was assembled on a $50 \times 50 \times 10$ mm base and an optical marker shown in Fig.1. The mock-up model consisted of two 20 mm diameter cylinders, two 8 mm diameter holes and four 10 mm holes.

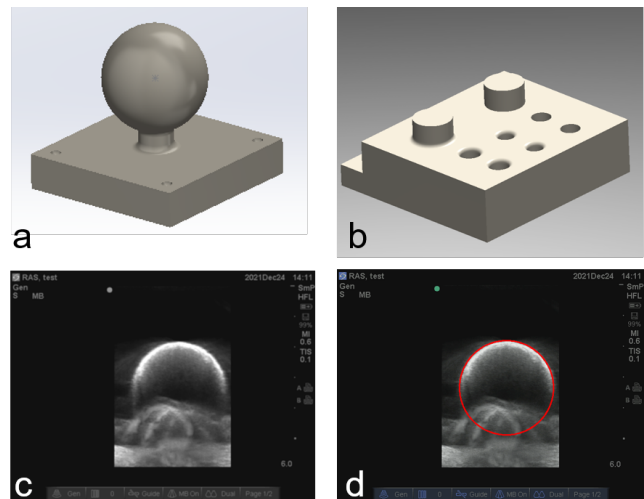


Fig. 3. (a) The sphere phantom for calibration and (b) mock-up model for robotic US reconstruction, (c) US image from the sphere phantom, (d) segmentation of sphere phantom with circle estimation.

During scanning of the mock-up model, the described motion profiles in SubSec.II-B were not used. Instead, the

US probe was held by the robot arm and kept perpendicular to the mock-up bottom surface. The US probe scanned along a predefined trajectory covering all geometric features in the mock-up model. The upper surface of the mock-up model was segmented from the recorded US images by image processing, and reconstructed with corresponding robot end effector poses by Eq.1. Finally, the mock-up surfaces were generated as point clouds and visualized by making use of the open source software cloudCompare (version 2.12).

III. RESULTS

A. Geometric Representation Error

During reconstruction, only the upper surface of the mock-up model was reconstructed to present the designed geometric features. The geometric representation errors of the different motion profiles are shown in Table III. Fig. 4 displays examples of the reconstructed point clouds from the proposed motion profiles. The absolute distance errors were quantified and illustrated by a colour scale. The RMSE of reconstructed model ranged from 0.27 to 0.69 mm according to the different motion profiles. The mean absolute errors ranged from 0.16 to 0.52 mm while the standard deviations were between 0.20 to 0.45. The average of RMSE from group *I*, *II* and *III* were 0.38, 0.48 and 0.52 mm respectively.

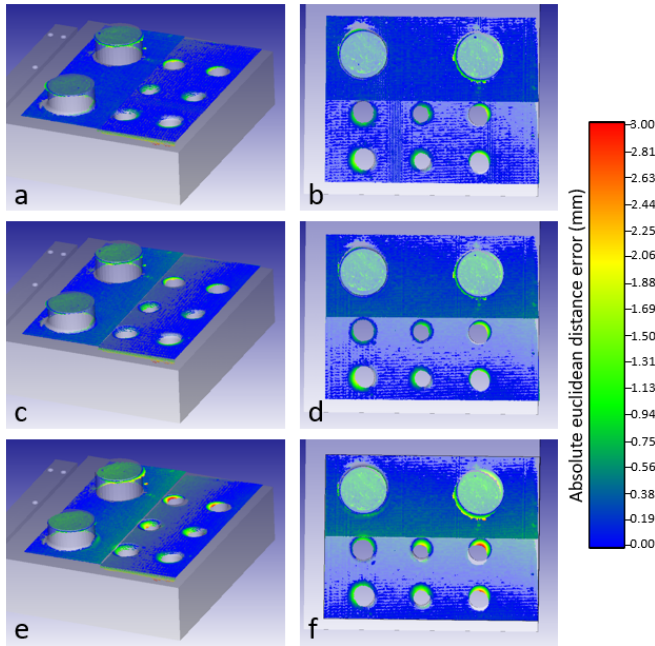


Fig. 4. 3D reconstructed point clouds of mock-up model (gray) with geometric representation errors. The Color scale illustrates the absolute euclidean distance error. (a) and (b) are reconstruction from motion profile 1, (c) and (d) are reconstruction from motion profile 4, (e) and (f) are reconstruction from motion profile 7.

B. 3D Localization Error

The 3D localization error represents whether the US calibration is able to produce a point cloud at the correct location in 3D space. Localization errors of the different motion profiles are shown in Table IV. The RMSE error for

TABLE III
GEOMETRIC REPRESENTATION ERRORS FROM DIFFERENT COMBINATION OF MOTION PROFILES. MEASUREMENTS ARE IN MILLIMETER.

Motion group	Motion Profile	RMSE	Mean	Std. Dev.
<i>I</i>	1	0.27	0.16	0.20
	2	0.42	0.21	0.26
	3	0.45	0.25	0.27
	Average 1-3	0.38	0.21	0.42
<i>II</i>	4	0.30	0.22	0.21
	5	0.35	0.24	0.26
	6	0.69	0.52	0.45
	Average 4-6	0.48	0.33	0.56
<i>III</i>	7	0.48	0.28	0.28
	8	0.56	0.32	0.39
	9	0.61	0.37	0.41
	10	0.43	0.26	0.33
	Average 7-10	0.52	0.31	0.71

motion group *I* ranges from 716.79 to 1767.22 mm. When rotation and translation are combined, such as motion group *II*, the RMSE is up to 2.42 mm while the mean error is up to 5.86 mm. Besides, by combining the motions in different Z axis, the results are not improved noticeably, as the average RMSE error of motion group *III* is around 2.28 mm and of *II* is around 2.31 mm respectively.

TABLE IV
3D LOCALIZATION ERRORS FROM DIFFERENT COMBINATION OF MOTION PROFILES. MEASUREMENTS ARE IN MILLIMETER.

Motion group	Motion Profile	RMSE	Mean	Std. Dev.
<i>I</i>	1	716.79	716.62	11.74
	2	864.40	864.09	22.91
	3	1767.22	1767.11	19.64
	Average 1-3	1213.78	1115.94	32.38
<i>II</i>	4	2.24	5.04	2.75
	5	2.27	5.16	2.51
	6	2.42	5.86	2.70
	Average 4-6	2.31	5.25	4.60
<i>III</i>	7	2.18	4.75	2.49
	8	2.31	5.31	2.31
	9	2.32	5.40	2.33
	10	2.30	5.30	2.33
	Average 7-10	2.28	5.19	4.73

IV. DISCUSSION

US image calibration is an important step to apply US in clinical scenarios. US image calibration provides accurate anatomic features to surgeons. However, the calibration outcomes are influenced by several factors such as calibration motion. There is no investigation in different calibration motion profiles in the past years. Therefore, this study compares the influence of calibration motions and also provides guidance on robotic US calibration procedures to ensure a high accuracy result.

In this paper, we proposed several scanning motions with a sphere phantom for robotic US image calibration. The image processing also impacts the calibration accuracy. The developed 3D sphere phantom is scanned as circles in 2D US images. With traditional image processing, the sphere contour is segmented and estimated accurately and automatically. The sphere phantom obtained fast image processing and precise

image segmentation comparing with conventional wire phantoms. Besides, the calibration motions were categorized as individually translation and rotation motions along sphere phantom coordinate. By applying different combinations of individual motions, the transformation matrix and scaling factor were computed. Then it was quantitatively assessed by using robotic 3D US reconstruction and visualized as point clouds.

The evaluation is built on two criteria: geometric representation error and 3D localization error. The geometric representation errors are slightly different among different groups. The reconstructed models are accurately reconstructed and matched with the mock-up model after registration in Fig.4. Motion profile 1, only translation along x and y axis at a single z axis position, results in accurate reconstruction. The z axis position to perform motion profile 1 does not matter, since motions 1, 2 and 3 yield similar results. It is observed that adding rotation around x and y axis to motion profile 1 and 2, does not yield better results than motion group *I* from Table III. The same applies for motion group *III*, since combining data from the motion group *II* does not improve the geometric representation error. The reconstructed model could provide an accurate shape and geometry feature with a 0.31 mm mean error which is better than the 0.69 mm from Rousseau [9]. These results present the capability and repeatability for representing geometric features, i.e. size and shape of the designed mock-up model.

Therefore, we believe that no additional motion is required to the translation along x and y axis, i.e. motion group *I*, in order to obtain accurate geometric representation. Thus, if the objective of US calibration is solely to obtain accurate 3D reconstruction of a target structure for medical image analysis or diagnostics, only performing a translational motion profile such as motions 1, 2 or 3 satisfies this objective.

In previous studies, only few of them evaluated the 3D localization error with reconstruction. By reconstructing a custom designed phantom, Ackerman *et al.* reported the mean error of the localization differences was up to 1.62 ± 1.28 mm with the freehand US calibration [17]. Besides, Li *et al.* reported the RMSE of 3D localization was up to 2 mm by applying a complex combination of translational and rotational motion with a robotic-assisted US system [10]. From the localization error in Table IV, it is observed that motion group *I* is not capable to produce a point cloud at the correct location in 3D space. Only when rotation motion is added, i.e. motion group *II*, the reconstructed point cloud is positioned accurately in space. Meanwhile, the z axis position to perform motion group *II* does not contribute to the calibration outcomes, since motions 4, 5 and 6 yield similar results. When combining these motions at different z axis positions, i.e. motion group *III*, the RMSE of 3D localization changes slightly and ranges from 2.18 to 2.32 mm. Therefore, the comparison of the aforementioned results reveals that if the objective of US calibration is to obtain accurate 3D volume reconstruction at the correct 3D space location, performing motion group *II* at a single z axis location is sufficient.

This paper proposed scanning motion profile is also adaptive to the other derivation of single point phantom, such as cross-wire phantom, with position control. It only requires an accurate alignment between the US probe and the phantom target point. The presented robotic scanning motions can also be manipulated for freehand calibration, however, the exact motion profiles will be harder to accomplish as accurately as robot-assisted calibration.

V. CONCLUSIONS

This paper compares the influence of different calibration motions by proposing several different calibration motion profiles. In this work, the properly combined translation and rotation motion presents an accurate anatomic volume with robotic 3D US reconstruction. This paper is the first one that investigate and provide optimal motion profile utilizing a minimum amount of motions. Future work should focus on decreasing the localization error. In addition, the motion range of individual motions can be increased depending on the experimental setting.

ACKNOWLEDGMENT

This project has received funding from European Union's Horizon 2020 research and innovation programme under grant agreement No.101016985 and Flemish Research Foundation (FWO) under grant agreement NO.G0A1420N and NO.1S36322N.

REFERENCES

- [1] A. Lasso, T. Heffter, A. Rankin, C. Pinter, T. Ungi, and G. Fichtinger, "Plus open-source toolkit for ultrasound-guided intervention systems," *IEEE Trans. Biomed. Eng.*, vol. 61, no. 10, p. 2527–2537, 2014.
- [2] Z. Jiang, Z. Li, M. Grimm, M. Zhou, M. Esposito, W. Wein, W. Stechele, T. Wendler, and N. Navab, "Autonomous robotic screening of tubular structures based only on real-time ultrasound imaging feedback," *IEEE Trans. Ind. Electron.*, pp. 1–1, 2021.
- [3] T. Ungi et al., "Navigated breast tumor excision using electromagnetically tracked ultrasound and surgical instruments," *IEEE Trans. Biomed. Eng.*, vol. 63, no. 3, p. 600–606, 2016.
- [4] Z. Chen and Q. Huang, "Real-time freehand 3d ultrasound imaging," *Comput. Methods Biomech. Biomed. Eng. Imaging Vis.*, vol. 6, no. 1, p. 74–83, 2019.
- [5] R. Li, C. Yuyu, K. Niu, and E. Vander Poorten, "Comparative quantitative analysis of robotic ultrasound image calibration methods," *20th International Conference on Advanced Robotics*, pp. 511–516, 2021.
- [6] M. H. Mozaffari and W.-S. Lee, "Freehand 3d ultrasound imaging: A systematic review," *Ultrasound Med. Biol.*, vol. 43, no. 10, p. 2099–2124, 2017.
- [7] P.-W. Hsu, R. W. Prager, A. H. Gee, and G. M. Treece, "Freehand 3d ultrasound calibration: A review," *Advanced Imaging in Biology and Medicine*, p. 47–84, 2009.
- [8] G. M. Treece, A. H. Gee, R. W. Prager, C. CASH, and L. Berman, "High-definition freehand 3-d ultrasound," *Ultrasound Med. Biol.*, vol. 29, no. 4, p. 529–546, 2003.
- [9] F. Rousseau, P. Hellier, M. M. J. Letteboer, W. J. Niessen, and C. Barillot, "Quantitative evaluation of three calibration methods for 3-d freehand ultrasound," *IEEE Trans. Med. Imaging*, vol. 25, no. 11, p. 1492–1501, 2006.
- [10] R. Li, K. Niu, and E. Vander Poorten, "A framework for fast automatic robot ultrasound calibration," *2021 International Symposium on Medical Robotics (ISMR)*, pp. 1–7, 2021.
- [11] F. Aalamifar, A. Cheng, Y. Kim, X. Hu, H. Zhang, X. Guo, and E. Boctor, "Robot-assisted automatic ultrasound calibration," *Int. J. Comput. Assist. Radiol. Surg.*, vol. 11, no. 10, p. 1821–1829, 2016.

- [12] E. L. Melvaer, K. Mørken, and E. Samset, "A motion constrained cross-wire phantom for tracked 2d ultrasound calibration," in *Int. J. Comput. Assist. Radiol. Surg.*, vol. 7, no. 4, 2012, p. 611–620.
- [13] K. Niu, J. Homminga, V. I. Sluiter, A. Sprengers, and N. Verdonschot, "Feasibility of a-mode ultrasound based intraoperative registration in computer-aided orthopedic surgery: a simulation and experimental study," *Plos One*, 2018.
- [14] E. Aertbelien and J. De Schutter, "etasl/etc: A constraint-based task specification language and robot controller using expression graphs," in *International Conference on Intelligent Robots and Systems*, 2014.
- [15] E. Chen, B. Ma, and T. Peters, "Quantitative assessments for ultrasound probe calibration," in *Medical Image Computing and Computer Assisted Intervention – MICCAI 2021*, p. 363–3724, 2021.
- [16] M. Sinko, P. Kamencay, R. Hudec, and M. Benco, "3d registration of the point cloud data using icp algorithm in medical image analysis," *2018 ELEKTRO*, pp. 1–6, 2018.
- [17] M. K. Ackerman, A. Cheng, E. Boctor, and G. Chirikjian, "Online ultrasound sensor calibration using gradient descent on the euclidean group," *2014 IEEE International Conference on Robotics and Automation (ICRA)*, 2014.